Case Study: Monitoring and modelling tidal-induced pore pressure oscillations in the soil of St. Mark's Square in Venice

Francesca Ceccato[1], Paolo Simonini[2] and Francesco Zarattini[3]

1 PhD. Affiliation: DICEA-University of Padua, via Ognissanti 39, 35129 Padua, Italy. corresponding author. E-mail: francesca.ceccato@dicea.unipd.it

2 Prof. Affiliation: DICEA-University of Padua, via Ognissanti 39, 35129 Padua, Italy

3 M.Sc. Affiliation: DICEA-University of Padua, via Ognissanti 39, 35129 Padua, Italy

Abstract

Sea level rise and high tide events are threatening many coastal cities, which require adequate and sustainable protection measures. The historic city centre of Venice (Italy) is often flooded during very high tide events, especially the area of St. Mark's island, which is at the lowest elevation among all the islands forming the city. In order to design cost effective protection interventions to safeguard the historical heritage, a deep understanding of flooding mechanisms and the relationship between groundwater pressure and tidal oscillations are necessary. Geotechnical survey and analyses play an important role in this process. This paper presents the results of a recent monitoring campaign carried out in St. Mark's island. A simplified one-dimensional analytical model has been derived for saturated conditions to understand the key parameters that govern tidal induced pressure oscillations in soil (material properties, geometrical features and wave properties). Additional features, such as partially saturated soil conditions and two-dimensional effects, have been investigated numerically. Results show that significant pressure oscillations occur in the subsoil, which should not be neglected for the stability of horizontal architectural structures, such as the historical mosaics and paving. However, seepage flow rate is small, thus its impact on the drainage system is limited in terms of water discharge.

Keywords: tidal pressure oscillations; pressure monitoring; seepage; coastal flooding.

Final paper can be downloaded at: https://ascelibrary.org/doi/10.1061/%28ASCE%29GT.1943-5606.0002474

Cite this work as: Ceccato, F., Simonini, P., and Zarattini, F. (2021). "Monitoring and Modeling Tidally Induced Pore-Pressure Oscillations in the Soil of St . Mark ' s Square in Venice , Italy." *Journal of Geotechnical and Geoenvironmental Engineering*, 147(5), 1–14.

INTRODUCTION

Extremely high sea levels have increased in frequency and magnitude in many coastal sites around the world due to climate change (Favaretto et al. 2019; Fritz et al. 2008; Vousdoukas et al. 2017). This will increase annual damage due to coastal flooding, thus large protection measures need to be undertaken in coastal areas to protect them from increasing sea level rise risks.

One of the most threatened cities is the world-famous historic city of Venice (Italy) situated on a group of low-lying islands in the northern part of the Adriatic Sea. Venice has been affected in the last 100 years by a significant increase in the frequency of flooding (Carbognin et al. 2010; Rinaldo et al. 2008). The lowest part of the city is St. Mark's Square, which is flooded several times a year for a few hours. This induces considerable deterioration of masonry walls, foundations and decorative architectural elements of buildings (Bettiol et al. 2015; Ceccato et al. 2014; Fletcher and Spencer 2005), jeopardizing the historical heritage.

In this peculiar context, finding the optimal solution to safeguard the historic city and the surrounding lagoon is complex because it must be respectful of the historical heritage, compatible with the touristic and economical activities of the most important site of the city and cost effective. The flood risk management strategies are being developed with a multidisciplinary, long-term perspective, and with a fruitful discussion between scientists, stakeholders and policy makers. This approach agrees with many recent studies, which point out that it is necessary to integrate innovative technical measures in a strategic policy context which also considers environmental, social and economic issues (Center 2009; Penning-Rowsell et al. 2014; Zanuttigh 2011; Zanuttigh et al. 2014).

Several alternative strategies have been considered in past years to protect the area (see next section), including renovation of the old drainage system, elevation of quay walls to prevent overtopping, as well as extensive vertical seepage cut-off walls driven along the island perimeter or a horizontal waterproofing membrane under the pavement. An efficient choice of the set of necessary mitigation measures requires a careful evaluation of the flooding mechanisms. This paper focuses on the geotechnical issues of this complex problem and, in particular, on the tidal induced pore pressures and seepage flow in the ground.

Groundwater level fluctuations in response to a tidal forcing were investigated by several previous authors, see e.g. Cola et al. (2008), Horn (2002), Sun (1997), Turner et al. (1997), Turner (1998), Ursino et al. (2004), with the main purpose of studying coastal erosion, flora and fauna habitat, and run-up on structures such as breakwaters. However, the case presented in this study considers a urban environment characterized by different boundary conditions compared to previous studies.

An extensive field investigation and survey was carried out, including geotechnical field and laboratory investigations to characterize the soils, and monitoring of pore pressures in the ground in order to evaluate their response to tidal oscillations. A simplified one-dimensional analytical model was derived to understand the key parameters of the phenomenon, considering water seepage in saturated soil through the boundary wall. Additional features such as partially saturated soil conditions, and two-dimensional effects, have been investigated numerically. The results show that the response is mainly governed by boundary conditions, soil hydraulic conductivity and partial saturation properties.

The outcome of the study not only provided important insights for a sustainable design of the measures to protect the historical area of St. Mark's Square, but also interesting information on the pore pressure evolution in the subsoil due to tidal oscillations, which could be useful for other coastal engineering applications.

VENICE AND "HIGH WATER"

Venice is situated in the northern part of a lagoon, which is approximately 50 km long, and 10 km wide located in the northwest part of the Adriatic Sea (Fig. 1). The lagoon has a complex bathymetry, and is characterized by a network of channels, small islands, tidal flats and marshes: the lagoon exchanges water with the Adriatic Sea through the three inlets of Lido, Malamocco and Chioggia, primarily controlled by the tide that normally has an amplitude between 0.40 m and 0.60 m and a period of 12 hours.

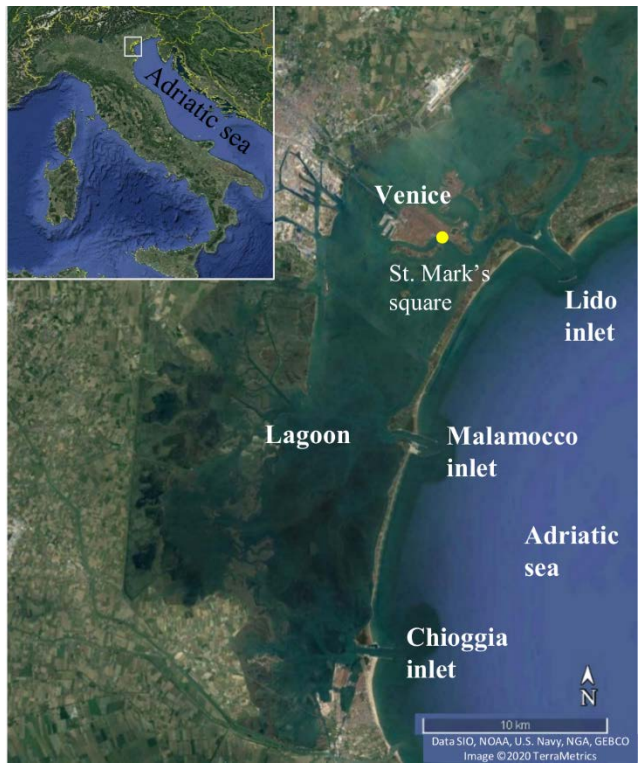

Fig 1. View of Venice Lagoon (Google Earth, Image © 2020 TerraMetrics)

As a consequence of eustacy, i.e. natural sea level rise, and subsidence, the city of Venice has "lost" 240 mm with respect to the sea, and floods have become more frequent and intense (Barbieri et al. 2007; Carbognin et al. 2010; Ricceri 2007; Rinaldo et al. 2008).

The term "*acqua alta*" (literally '*high water*') indicates the phenomenon in which, during particularly high tides, sea water can partially flood the historic city centre. Very high water levels are generated by the superposition of the astronomical tide with storm surge. For the city of Venice, this latter contribution is particularly relevant when intense winds blow in from South-East (named *Scirocco* direction). Very high water levels cause significant impact in city services and, in some exceptional cases, great property damage.

A long-term safeguarding project, covering a wide range of engineering measures for erosion mitigation, morphological restoration of the coastline, and artificial elevation of some islands was

launched. The most significant and challenging element in such a far-ranging plan of countermeasures is represented by the ambitious MOSE project, consisting in a series of mobile barriers for the temporary closure of the lagoon inlets in case of very high tides (https://www.mosevenezia.eu/, Jamiolkowski et al. 2009).

Measurement and prediction of the tidal excursion in Venice are relative to the local tidal reference named "*Zero Mareografico di Punta Salute*" (zero mareographic level of Punta Salute, ZMPS), that is located at +0.236 m above the mean sea level. In Venice, a tide higher than +0.80 m above ZMPS, also indicated as *m s.l.P.S.*, is conventionally referred as to "*acqua alta*". When the tide exceeds +1.00 m, 5% of the islands is flooded (it occurred 654 times between 1966 and 2019, https://www.comune.venezia.it/); this percentage increases to 59% when it reaches +1.40 m (it occurred 22 times between 1966 and 2019, https://www.comune.venezia.it/).

St. Mark's Square has an average elevation between +0.80 m and +0.90 m s.l.P.S. Some parts, namely the narthex of St. Mark's Basilica, are located at an even lower level, at +0.60 m s.l.P.S. Fig. 2 shows a pictorial view of the St. Mark's area with the locations inundated when the sea level reaches specific values. When the water level reaches +0.60 m, it starts inundating a small zone in front of the Basilica and its narthex (on average it occurred 361 times a year between 1999 and 2016). With a water level of 0.90m, approximately 65% of the square is flooded and with a level of 1.15m it is completely submerged (on average it occurred 18 times a year between 1999 and 2016).

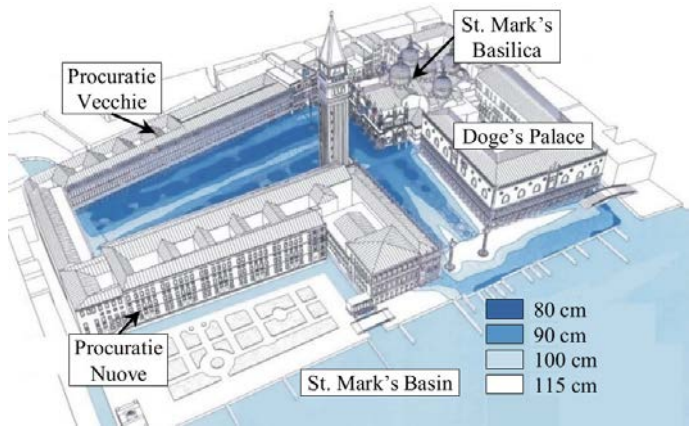

Fig 2. View of St. Mark's island with areas inundated at corresponding values of tidal levels (modified from CVN, 2020)

To ensure frequent water exchange between the lagoon and the Adriatic Sea, the closure of the inlets through the MOSE gates will occur only when a sea level exceeding +1.10 m s.l.P.S. or higher is forecast, thus flooding of the historical area of St. Mark's Square is unavoidable and specific protection measures are necessary.

Fig. 3 depicts the main flooding mechanism of the square:

1. Back-flow through the drainage system composed of a complex network of embedded masonry tunnels, locally referred to as "*gatoli*", (Fig. 4) built in different historical periods and laying in various states of preservation;
2. Overtopping and overflow from the St. Mark's basin;
3. Heavy rainfalls occurring simultaneously with high sea levels;
4. Seepage through the soil below the paving and the permeable joints between the stone elements.

Mechanisms 1-3 have been investigated in specific hydraulic and maritime studies (P. Salandin 2020; Ruol et al. 2020) , which will not be discussed in this paper.

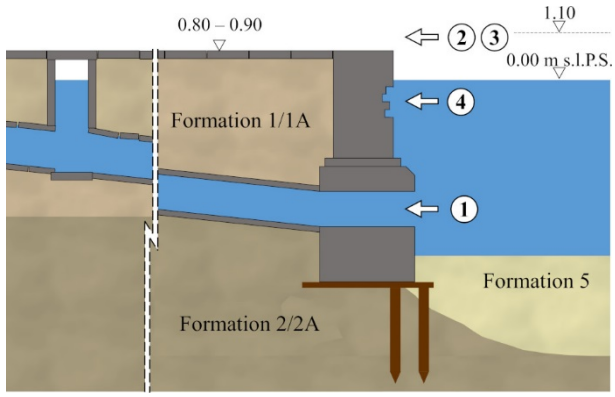

Fig 3. Main flooding mechanisms of St. Mark's Square: 1. Back-flow through the drainage system, 2. Overtopping, 3. Heavy rainfalls, 4. Seepage through the soil.

To prevent flooding due to mechanism 1, special valves will be installed in all the retrofitted active *gatoli*, to close the entire drainage system in correspondence of very high tide. Overtopping due to wind-induced waves will be controlled by installing special permanent floating barriers at some distance from the quay wall facing the St. Mark's basin. Mechanism 3 will be controlled by an automatic pumping system removing the rainfall water collecting by the drainage network to a storage tank built up below a new wharf.

Mechanism 4, which is related to some of the most expensive technical solutions (e.g. seepage cut-off, impermeable membrane), required a detailed geotechnical study, which is presented and discussed in this paper.

In order to avoid water infiltrating through and below the quay walls, the construction of vertical cut-off sheet pile wall around the boundary of the St. Mark's island was initially recommended. This is however a very expensive intervention, thus its implementation was considered necessary only if a significant amount of water is expected to enter by mechanism 4 that would be difficult to drain out with other techniques. The installation of an impermeable membrane below the stone pavement was also examined in preliminary project proposals in order to avoid seepage flow through the permeable joints between the stone elements. In the context of St. Mark square, this solution was discarded because the

oscillating tide-induced pore water pressure built up in the subsoil under the membrane could affect its long term effectiveness as well as the pavement stability, as it will be demonstrated in the following sections. The results presented in the following will prove, in fact, that these expensive protection measures are not necessary.

SITE INVESTIGATIONS

In 2018 *Consorzio Venezia Nuova* (CVN, the contractor in charge of the protection measures), commissioned detailed historical and archaeological studies to collect information on the evolution of the morphology of the St. Mark's island as well as an extensive site investigation campaign.

In order to define the geotechnical model of the subsoil, and given the complexity of the system, data from previous campaigns in the years 1993 and 1997 (CVN 1998) were enhanced by new data collected in 2019. In particular, the most recent geotechnical site investigation consisted in geotechnical boreholes up to a depth of 20 m; Piezocone Penetration Tests (CPTU); Seismic Piezocone Penetration Tests (SCPTU) with dissipation tests; Dilatometer tests (DTM); Seismic Dilatometer tests (SDTM) and field permeability tests. Geotechnical laboratory tests included classification tests (grain size distribution, specific gravity, water content, Atterberg limits, ect.), permeability tests in triaxial cell, with constant head and variable head permeameters and one-dimensional oedeometric compression tests.

Monitoring instrumentation (1 barometer, 4 tide gauges, and 25 piezometers) were installed to measure, respectively, atmospheric pressure, sea water level and pore pressure oscillation with time. The locations of the tests and instruments are shown in Fig. 4.

The position, dimensions and state of preservation of the elements constituting the drainage system were assessed correlating archaeological data with the results of electric tomography (ERT) and Georadar investigations as well as performing video inspections.

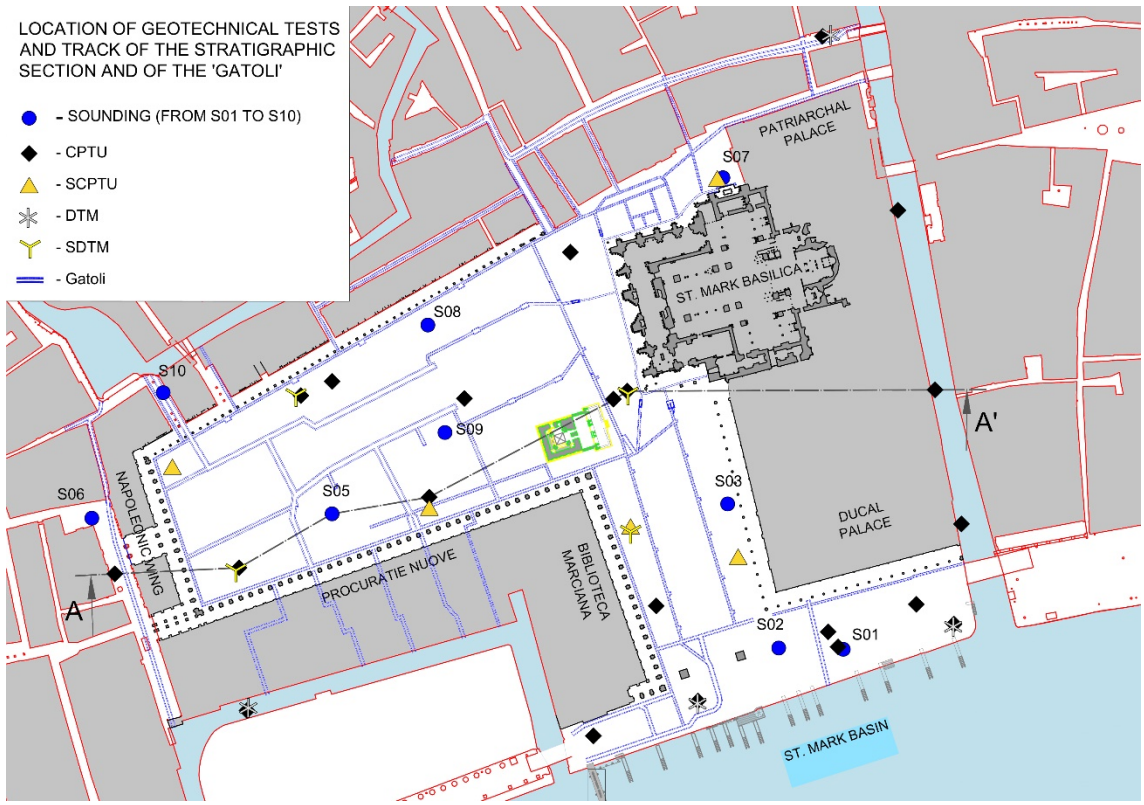

Fig 4. Position of in-situ geotechnical tests (CPTU, SCPTU, DMT, SDMT), piezometric stations (S01-S10) and *gatoli* network

Soil profile

The main characteristic of the Venice lagoon soils is the presence of a predominant silt fraction, combined with clay and/or sand to form highly heterogeneous deposits (Cola and Simonini 2002; Monaco et al. 2014; Ricceri et al. 2002; Simonini et al. 2007). The soils have been classified according to the Unified Classification System (USCS) and belong to the classes SM-SP, ML, and CL, or to a mixture of these classes (Tab. 1). The island of St. Mark is no exception; moreover, the shallowest layer, the most relevant to achieve the objectives of this study, experienced a number of different anthropic actions along with the centuries (Bortoletto 2019).

Table 1 summarizes the identified soil formations and Fig. 5 shows a typical soil profile derived from all available data of geotechnical site investigations (years 1993, 1997, 2019). Under the shallowest layer (1, 1A), reaching at most the depth of -3.20 m s.l.P.S., and with the characteristics of an anthropic fill, a low permeability layer (from sandy silt (2) to clayey silt (2A)) has been identified. Beneath this layer there is a more permeable sandy formation (3 or 3A), whose thickness varies from 0.50 m to approximately 8.00 m. From the depth of -9.80 m s.l.P.S., up to the maximum sounding depth, there is the typical alternation of prevalently clayey layers (4A) with lenses of moderately silty sand (4). Formations (1) and (1A), due to their anthropic nature are the most heterogeneous and their hydraulic conductivity varies across 4 orders of magnitude (Tab. 1).

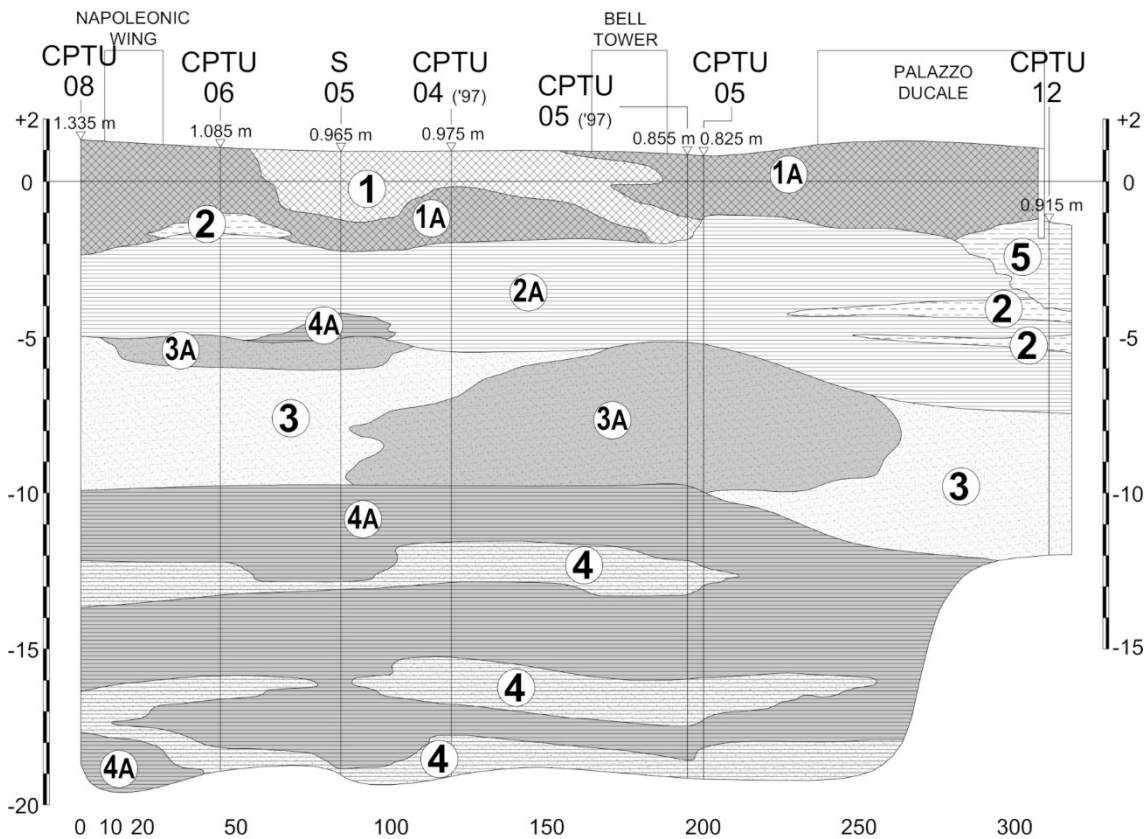

Fig 5. Typical stratigraphic section of St. Mark's Island (Section AA' in Fig. 3)

Table 1. Description of soil layers in St. Mark's area

Formation	Description	Hydraulic conductivity [m/s]
1	Anthropic fill layer. Heterogeneous material. Prevalently sandy material (SP or SP-ML), with inclusions of sandy silt, graveled sand, bricks, shell remains, wood remains.	$2.4 \times 10^{-4} \div 2.2 \times 10^{-6}$
1A	Anthropic fill layer. Prevalently silty heterogeneous material (ML), with inclusions of shells, wood and vegetal fibres; pebbles and bricks	$1.0 \times 10^{-6} \div 5.3 \times 10^{-8}$
2	Silt (ML) and sandy silt (ML-SP) with vegetal fibres, peat traces and shells	$2.4 \times 10^{-7} \div 2.0 \times 10^{-8}$
2A	Clayey silt (ML-CL) with vegetal fibres, peat traces and shells	$7.8 \times 10^{-8} \div 5.3 \times 10^{-9}$
3	Fine sand (SP)	$3.4 \times 10^{-6} \div 2.2 \times 10^{-6}$
3A	Silty sand (SP-SM) with clayey silt lenses (ML-CL)	$2.9 \times 10^{-6} \div 2.0 \times 10^{-7}$
4	Silty sand (SM) and sandy silt (ML-SP)	$2.6 \times 10^{-6} \div 1.3 \times 10^{-6}$
4A	Clay (CL) with clayey silt lenses (ML-CL)	$2.5 \times 10^{-8} \div 3.5 \times 10^{-9}$
5	Mud from the bottom of the canal	
6	Heterogeneous formation: sand, silt and clay	

The drainage network

The ancient drainage system of the historic city as well as of St. Mark's Square was mostly designed and constructed in the 18th century and is still functioning. It is composed of a network of smaller and larger masonry tunnels (*gatoli*) embedded in the anthropic formation (1 and 1A), gently sloping towards the surrounding canals (Fig. 4). The tide flows in and out from the *gatoli* network fostering sediment deposition, thus reducing their effective section to 50-75% with time (Volpato 2019). *Gatoli* of smaller size are commonly characterized by an inner 0.40-0.80 m-wide and 0.60-1.30 m-high rectangular section. They were constructed with 0.30 m-thick masonry lateral walls and closed on top by a gray platy stone referred to as *stelere* as shown in Fig. 6a. Wider sections feature a masonry vault and can reach a width of 1.50 m (Fig. 6b). Due to this construction system, the drainage network is not fully impermeable, thus infiltration across the walls and through the fissures between the upper *stelere* and the lateral walls is possible.

Their state of preservation and effective section was assessed by video inspection during very low tidal levels, showing that in some cases the mortar between masonry elements has significantly deteriorated, and for this reason they are even more permeable. Preliminary hydraulic measurements and models (Volpato 2019) show that the hydraulic head inside the *gatoli* coincides with the sea water level, i.e. the system is well connected to the sea and water flows in and out rapidly according to tidal fluctuation .

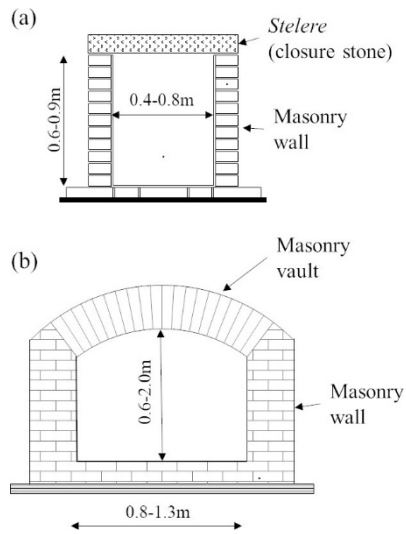

Fig 6. Typical cross section of Venetian *gatoli*

PORE-WATER PRESSURE READINGS

During the first months of 2019, 25 piezometers were installed on 10 monitoring sites distributed in the whole of St. Mark's Square as shown in Fig. 4 (S01 to S10). According to the local conditions, it was decided to use 2 or 3 piezometers for each station, measuring the absolute pore water pressure in the different formations (1, 2 or 3).

Fig. 7 provides an example of the position of the piezometers in the station. The upper and the lower piezometer, labelled respectively Pz. A and Pz. B, are installed in the more permeable formations (1) and (3). These are standpipes with a 1 m-long filtration section; the gap between the borehole and the pipe has

been properly sealed in order to prevent hydraulic communication between different aquifers. In five of the ten stations, an intermediate piezometer (Pz. C, Casagrande type) is located in the less permeable formation (2). Pressure oscillations in this layer are very small and will not be discussed in this paper.

The head of all the piezometers has been capped and sealed to prevent any contact with the surrounding environment in order to avoid the submerging tide affecting the water pressure readings.

The measurements of groundwater pressure in different positions and depths provided interesting information about the tide propagation in the subsoil.

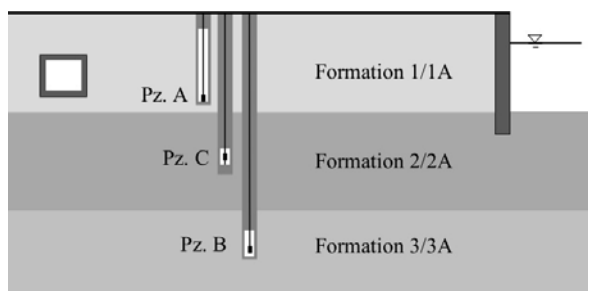

Fig 7. Schematic representation of piezometer position is a station

Fig. 8 shows a typical result of the piezometer readings installed in permeable formations (1) and (3) compared with the sea level fluctuation.

The response is relatively different from site to site due to the subsoil heterogeneity and boundary conditions, but some common features may be noticed and summarized as follows:

- The average water level in both layers (1) and (3) is higher than the average sea level. This is probably due to the effect of different additional contributions such as rainfall, anthropic water discharge, infiltrations at far boundary, etc. that have also been observed in previous studies (Cola et al. 2008; Di Sipio and Zezza 2011);
- At higher tides, higher water levels are observed in the shallower layer (1) compared to the deeper layer (3), thus the hydraulic gradient is directed downwards; on the contrary at lower tide levels, lower

groundwater levels are observed in layer (1) with respect to layer (3) and therefore the hydraulic gradient is directed upwards;

- In the shallower layer, maximum piezometer levels are close to sea level, whereas the minimum ones stay significantly higher than sea level, suggesting a sudden response at sea level rising and a delayed response during its decrease. This observation is in agreement with the pore pressure measurements in salt marshes by Cola et al. (2008).

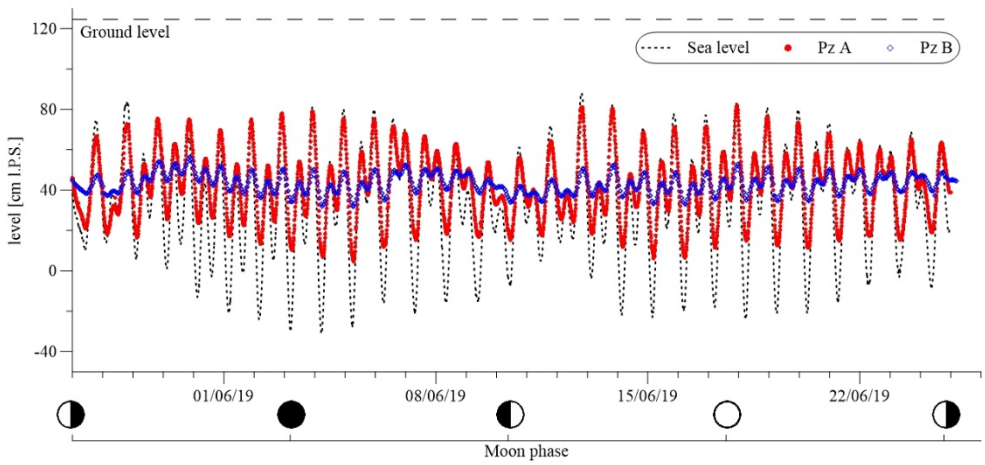

Fig 8. Sea level and piezometric level (S06) from 27-05-2019 to 25-06-2019

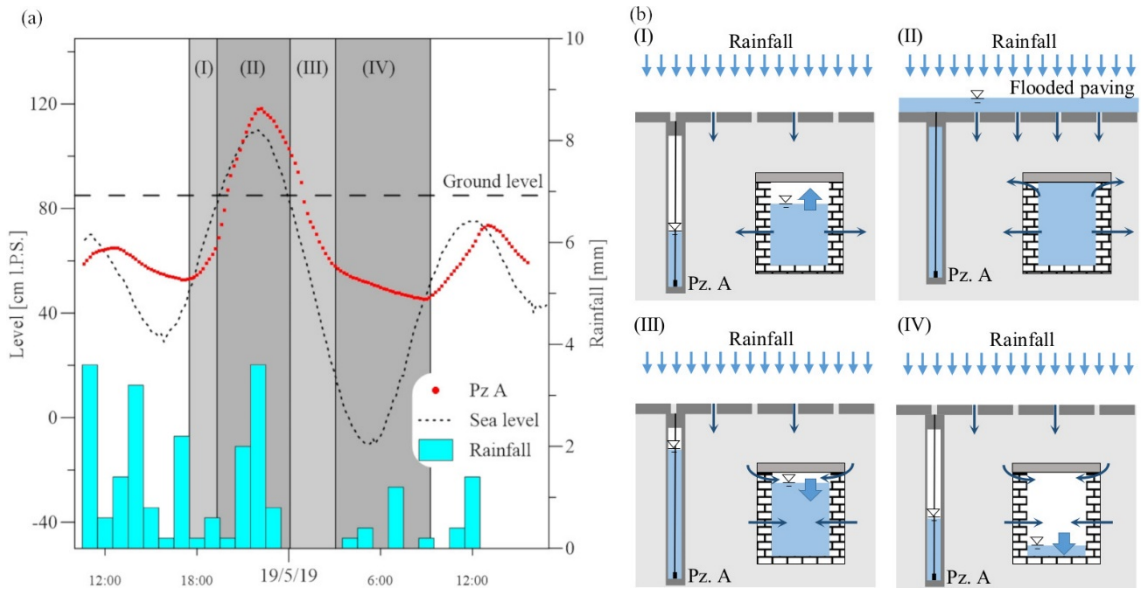

Fig 9. (a) Sea level, piezometric level (S08) and hourly precipitation (courtesy of Centro Previsioni e Segnalazioni Maree, Venezia) the 19-05-2019. (b) Schematic representation of water flow in phases I, II, II and IV indicated in subfigure a.

Local soil heterogeneities, distance from perimeter quay walls and the *gatoli* network, as well as their geometric features and state of preservation, influence significantly the hydraulic response of the entire subsoil system.

A typical pore pressure response in formation (1) as a function of sea level and hourly rainfall is shown in Fig. 9 for piezometer S08-A. Ground level at this location is +0.86 m and the area is frequently flooded during high tide. Piezometer oscillation is attenuated and delayed compared to tidal oscillation as better discussed in the following sections.

When the tide rises, water enters the *gatoli* and can infiltrate into the soil though their permeable walls, as shown in phase (I) of Fig. 9. A certain amount of rainfall water can also flow through the fissures in the permeable pedestrian paving made of rectangular 0.20 m thick grey stones. When the paving becomes submerged, i.e. in phase (II), pressure response is very fast because a larger seepage from the top boundary may occur. This fast response was also observed in salt marshes subjected to

submerging tides by Cola et al. (2008). The maximum piezometric level may eventually be higher than maximum sea level, as a consequence of some other significant contributions, such as rainfall or anthropic sources.

When the tidal level decreases, the pressure remains higher than the sea level because of the slow drainage response. This is an important fact to consider when carrying out uplift analyses of architectural elements such as the mosaics in the floor of the basilica. Initially, water drains out mainly from the walls of the *gatoli* (phase III), and then, for very low tide level, only from quay walls or very deep ducts, as in phase (IV) showing a slower pressure dissipation rate. In phase (IV) the soil may reach partially saturated conditions, thus reducing its permeability.

It is also interesting to compare the maximum piezometer level with the maximum sea level for several tidal periods, by calculating the oscillation attenuation factor ($IA = h_{i,max}/h_{tide,max}$, where i=A or B indicates the upper or lower piezometer) and delay factor ($IR = t_{i,max} - t_{tide,max}$).

This is done in Fig. 10 for station S01 lying very close to the quay wall facing St. Mark's Basin. The trend IR-IA is characterized by a very large scatter, but with some significant difference between the upper and the lower permeable formations. In the first case (piezometer A, red dots), the attenuation clearly decreases with increasing delay; on the contrary for the deeper sand deposit (blue circles), the attenuation remains relatively constant and not dependent on the delay. In the graph, a continuous line obtained from an analytical approach described in the following section is superimposed on the experimental data. Considering the relevant heterogeneity of the ground and the complex site boundary conditions, the analytical solution may give a reasonable explanation of the observed trend in the upper formation.

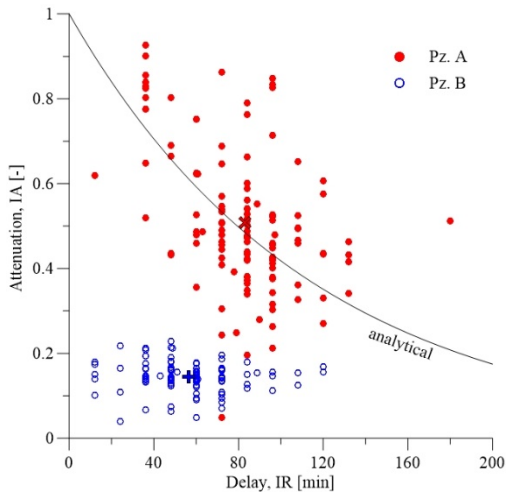

Fig 10. Attenuation and delay for piezometers of station S01, cross symbols indicate the average values.

ONE-DIMENSIONAL ANALYTICAL MODEL OF TIDAL INDUCED PRESSURE OSCILLATIONS

This section presents an analytical model for pore pressure oscillations in soil due to harmonic loading at the boundary to interpret the experimental measurements. The model considers a semi-infinite layer of homogeneous saturated soil; thus one-dimensional conditions can be assumed (Fig. 11). It can represent the case of a long soil layer subjected to a non-submerging tidal oscillation at its vertical end (e.g. a permeable quay wall).

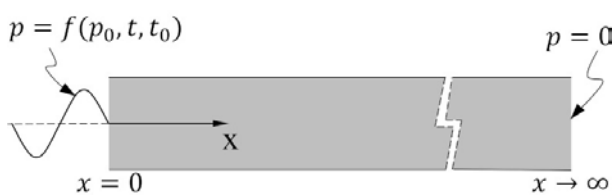

Fig. 11 Boundary conditions of the 1D analytical model

The model is developed considering the mass balance equations of the fluid inside the soil (Eq. 1).

$$\frac{\partial(\rho_L q)}{\partial x} = -\frac{\partial(\rho_L n S_L)}{\partial t} \qquad (1)$$

where ρ_L=liquid density, q=specific discharge, n= soil porosity and S_L= soil degree of saturation.

Assuming negligible liquid density gradients, the validity of Darcy's law and the Bernoulli equation, the term on the left-hand-side can be written as Eq. 2.

$$\frac{\partial(\rho_L q)}{\partial x} = \frac{\partial}{\partial x}\left(-\frac{k}{g}\frac{\partial p}{\partial x}\right) \quad (2)$$

where k is the hydraulic conductivity and $\underline{g}$ is gravity.

The time derivative at the right-hand-side of Eq. 1 can be written as Eq. 3

$$\frac{\partial(\rho_L n\, S_L)}{\partial t} = nS_L\frac{\partial \rho_L}{\partial p}\left(\frac{\partial p}{\partial t}\right) + \rho_L n\left(\frac{\partial S_L}{\partial p}\right)\left(\frac{\partial p}{\partial t}\right) + \rho_L S_L\frac{\partial n}{\partial t} \quad (3)$$

The derivative of density with respect to pressure is given by the state equation of the liquid. The derivative of the degree of saturation with respect to the pressure is given by the soil-water retention curve (SWRC), but in this case it is neglected as the soil is assumed to be fully saturated; the effect of this term in partially saturated soil is discussed in the next section where the seepage equation is solved numerically by FEM. The time derivative of the porosity is a function of the constitutive behaviour of soil, but for small oscillations, as considered in this case, this term is negligible compared to the others.

For saturated soil, the right-end-side of Eq. 1 can be written as:

$$-\frac{\partial}{\partial t}(\rho_L n\, S_L) = -\frac{n\rho_L}{K_L}\frac{\partial p}{\partial t} \quad (4)$$

Where K_L is the bulk modulus of the liquid in the soil.

Combining eq. 2 and 4 the mass balance equation becomes:

$$\frac{k}{\gamma_L}\frac{\partial^2 p}{\partial x^2} = \frac{n}{K_L}\left(\frac{\partial p}{\partial t}\right) \quad (5)$$

This differential equation can be integrated under the following boundary conditions:

$p = p_0\, sin\left(\frac{2\pi t}{t_0}\right)$ for x=0

p=0 for $x \rightarrow \infty$

$p_0 = \gamma_L h_0$ is the amplitude of the pressure oscillation induced by a tidal wave of amplitude h_0, and t_0 is the period of the oscillation.

The solution of the equation has the form

$$p = p_0 e^{-\frac{x}{\lambda}} sin\left(\frac{2\pi t}{t_0} - \frac{x}{\lambda}\right) + C \quad (6)$$

where

$$\lambda = \sqrt{\frac{kK_L t_0}{\pi n \gamma_L}} \quad (7)$$

and C is a constant. The normalized amplitude of the oscillation decreases with the distance x from the boundary as Eq. 8. It can be noted that the wave amplitude is smaller than 2% for a normalized distance $x/\lambda > 4$.

$$\frac{p}{p_0} = e^{-\frac{x}{\lambda}} \quad (8)$$

The delay of the wave can be expressed as Eq. 9

$$\frac{t_r}{t_0} = \frac{x}{2\pi\lambda} \quad (9)$$

Fig. 12 plots the normalized amplitude and the delay t_r in minutes for the typical parameters of the case study considered (t_0=12h n=0.4 $\gamma_w = 9.81\ K_L/n = 3.75GPa$). Amplitude decreases very rapidly according to decreasing hydraulic conductivity. In very permeable soils, e.g. k=10^{-3}m/s, pressure oscillation propagates with less attenuation and time delay (Fig.13a); while in low permeability soils, e.g. k=10^{-7}m/s, oscillations are negligible after a relatively short distance (Fig. 13b).

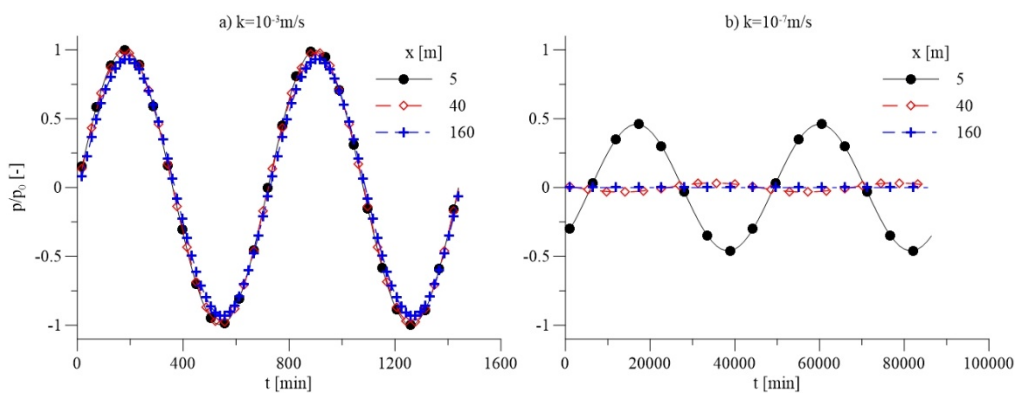

Fig 12. Analytical dimensionless amplitude (p/p_0)(a) and delay (t_r) (b) with distance (x) for different hydraulic conductivity.

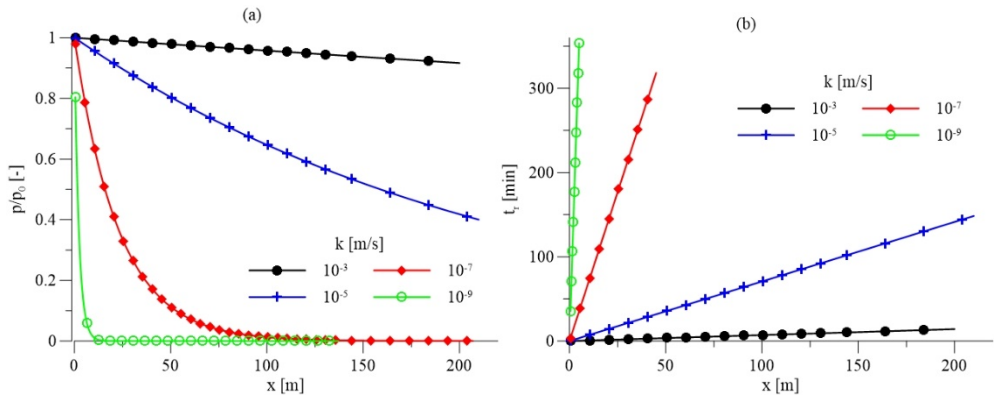

Fig 13. Analytical dimensionless amplitude (p/p_0) with time at different distances in case $k=10^{-3}$m/s (a) and $k=10^{-7}$m/s (b)

NUMERICAL MODELLING

In this section, seepage analysis carried out with FEM code Midas GTS-NX (v2019.2) is used to investigate the effects of partial soil saturation, different types of boundary conditions, and two-dimensional effects. Firstly, seepage from the quay wall is considered and secondly seepage from a *gatolo* is discussed.

Soil is assumed to be isotropic and linear elastic. Young's Modulus for the shallow anthropic layer is estimated on the basis of CPTU and laboratory test interpretation according to Biscontin et al. (2007) and Tonni and Simonini (2013) and set to E=100 MPa, whereas Poisson's ratio is reasonably equal to ν=0.3. Void ratio was assumed e=0.8 and hydraulic conductivity k varying between 10^{-3} m/s and 10^{-9} m/s.

The SWRC is estimated from the basic soil properties with the procedure explained in Aubertin et al. (2003). For coarse-grained materials it is estimated as a function of the grain size distribution, while for fine-grained materials it also depends on the liquid limit. A very large number of grain size distributions and Atterberg limits of the superficial layer were collected during geotechnical survey, from which three characteristic SWRCs have been derived (Fig. 14). The first curve (blue triangles) is typical of uniform sand (SP); the second (black dots) is typical of silty sand (SP-ML); the third one is typical of silty clay

(CL-ML). the Hydraulic conductivity curve (HCC) is estimated with the approach proposed by Mualem (1976) (Fig. 15).

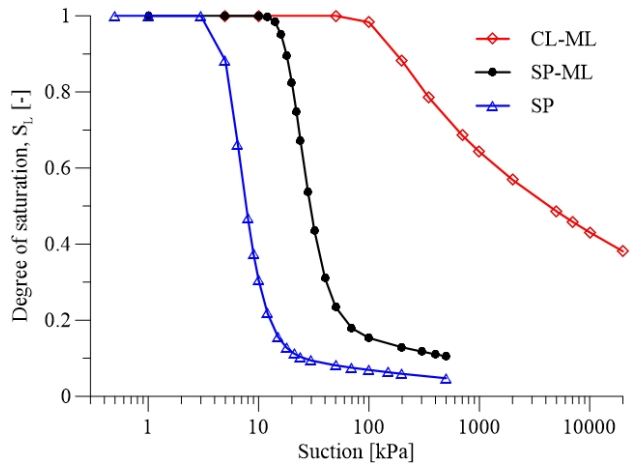

Fig 14. reference SWRC used in the numerical models for different soil types.

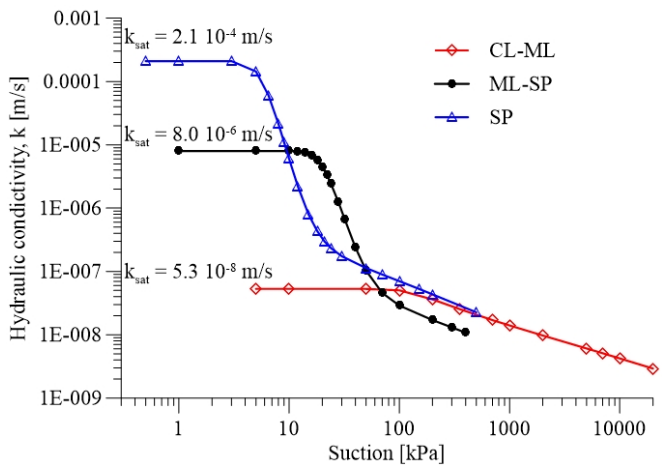

Fig 15. reference HCC used in the numerical models for different soil types.

Infiltration from quay wall

A thin layer of homogeneous soil in the FE model is assumed to schematize the anthropic formation (1). The elevation of the top and the bottom boundary are at y=+0.80 m and y=-2.00 m with respect to

ZMPS; the length of the mesh is 220 m (x and y are the horizontal and vertical coordinates respectively). The bottom boundary is impervious, to simulate the clayey-silty formation (2) (Fig. 16a).

The initial water level condition is assumed at 0.0m s.l.P.S. over the entire seepage field and then a sinusoidal tidal wave with an amplitude of 1.10 m and a period of 12 h is applied in terms of hydraulic head at the left boundary to simulate the typical water level oscillation in the lagoon.

The paving of St. Mark's Square is made of blocks of hard dark stone; however, it is not fully impermeable as water can flow through the space between blocks. To investigate the effect of its permeability, the top boundary of the model (paving) is either considered fully impermeable (case 1, Fig. 16a) or fully permeable (case 2 and 3). Moreover, when it is permeable, the surface is considered dry (case 2, Fig. 16b), thus water can flow out from this surface at atmospheric pressure, or flooded (case 3, Fig. 16c) by assuming a hydraulic head applied at the top boundary inducing downward water infiltration into the soil from this boundary.

For each case schematized in Fig. 16, three different types of soils have been considered with the properties listed in the previous section (SP, SP-ML, CL-ML). Moreover, each soil is either considered entirely saturated (SAT), i.e. partial saturation effect is not included in the governing equations of the model, or (eventually) unsaturated (USAT). This results in a total of 18 numerical simulations as summarized in Table 2. The most important outcomes of these parametric analyses are discussed in the following.

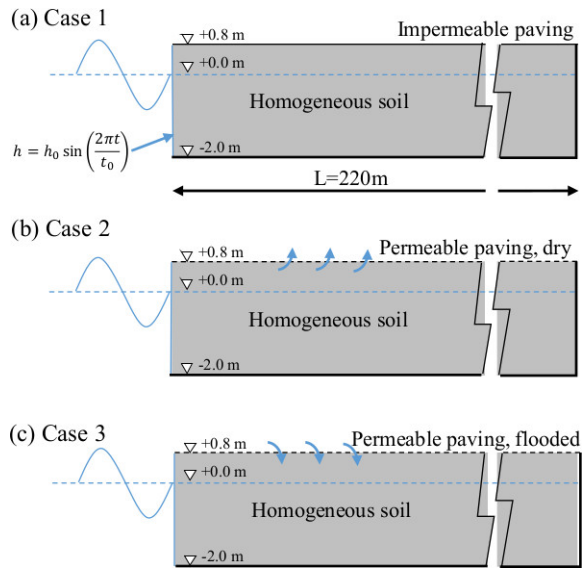

Fig 16. Geometry and boundary conditions of the numerical model considering infiltration from the quay wall (a) Case 1, (b) Case 2, (c) Case 3.

Table 2 Summary of numerical simulations considering infiltration from the quay wall

Boundary condition	Soil type	Saturated/Unsaturated	Simulation ID
Case 1	SP	Saturated	1-SP-SAT
		Unsaturated	1-SP-UNSAT
	SP-ML	Saturated	1-SPML-SAT
		Unsaturated	1-SPML-UNSAT
	CL-ML	Saturated	1-CLML-SAT
		Unsaturated	1-CLML-UNSAT
Case 2	SP	Saturated	2-SP-SAT
		Unsaturated	2-SP-UNSAT
	SP-ML	Saturated	2-SPML-SAT
		Unsaturated	2-SPML-UNSAT
	CL-ML	Saturated	2-CLML-SAT
		Unsaturated	2-CLML-UNSAT
Case 3	SP	Saturated	3-SP-SAT
		Unsaturated	3-SP-UNSAT
	SP-ML	Saturated	3-SPML-SAT
		Unsaturated	3-SPML-UNSAT
	CL-ML	Saturated	3-CLML-SAT

	Unsaturated	3-CLML-UNSAT

Fig. 17 shows the effect of considering partial saturation effects in uniform sand. Total head (triangles) and degree of saturation (circles) are plotted as functions of time for the saturated soil (black line, 1-SP-SAT), and the unsaturated soil (red lines, 1-SP-UNSAT). Considering partial saturation effects, the response of the system significantly changes because in Eq. 3 (i) the permeability decreases according to the HCC, (ii) the derivative of the degree of saturation is non-zero, and (iii) the degree of saturation is smaller than 1.

In the superficial zone, e.g. y=+0.6 m (Fig. 17a and b), soil becomes unsaturated, thus its hydraulic conductivity significantly decreases and the total head oscillation is substantially attenuated and delayed compared to the saturated case. When soil is saturated the response of the system is rapid, while the decrease of pore pressure is slower in partially saturated conditions. This is consistent with the monitoring data as shown in Fig. 9. At larger depths, e.g. y=-2.0 m (Fig. 17c and d), soil remains essentially saturated, but since the hydraulic conductivity of the system is lower than the saturated case the attenuation and delay are larger than the saturated case at longer distances from the quay wall.

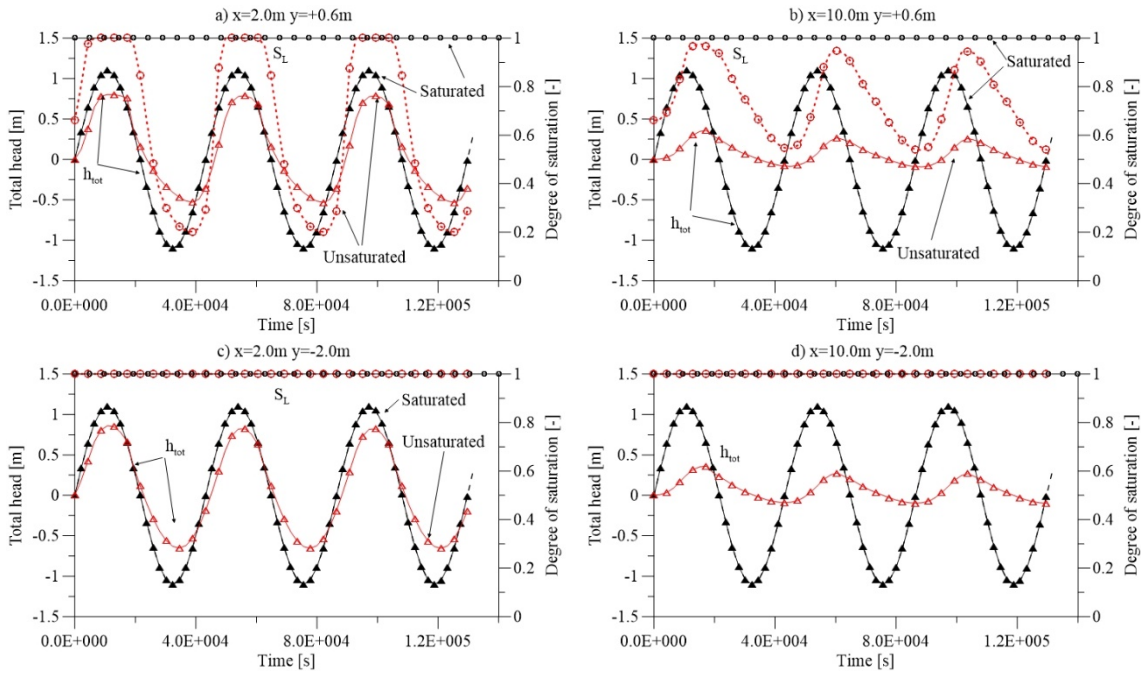

Fig 17. Total head and degree of saturation along time at four different points for 1-SP-SAT and 1-SP-UNSAT (a) x=2.0m, y=+0.6m; (b) x=10.0m, y=+0.6m; (c) x=2.0m, y=-2.0m; (d) x=10.0m, y=-2.0m.

Fig. 18 shows the oscillations of total head and the degree of saturation at x=10m, y=+0.6m for typical soil types composing the anthropic layer. In saturated conditions (Fig. 18a), attenuation and delay are essentially governed by hydraulic conductivity as observed in the previous section, thus they are maximum for silty clay (CL-ML) and minimum for uniform sand (SP). In contrast, since not only hydraulic conductivity, but also the slope of the SWRC and the degree of saturation play a relevant role (see eq. 3), the response is more complex in partially saturated conditions (Fig. 18b, c). Uniform sand experiences a low degree of saturation, low hydraulic conductivity and the slope of the SWRC is high; for these reasons the reduction of wave amplitude and delay is higher than other soils.

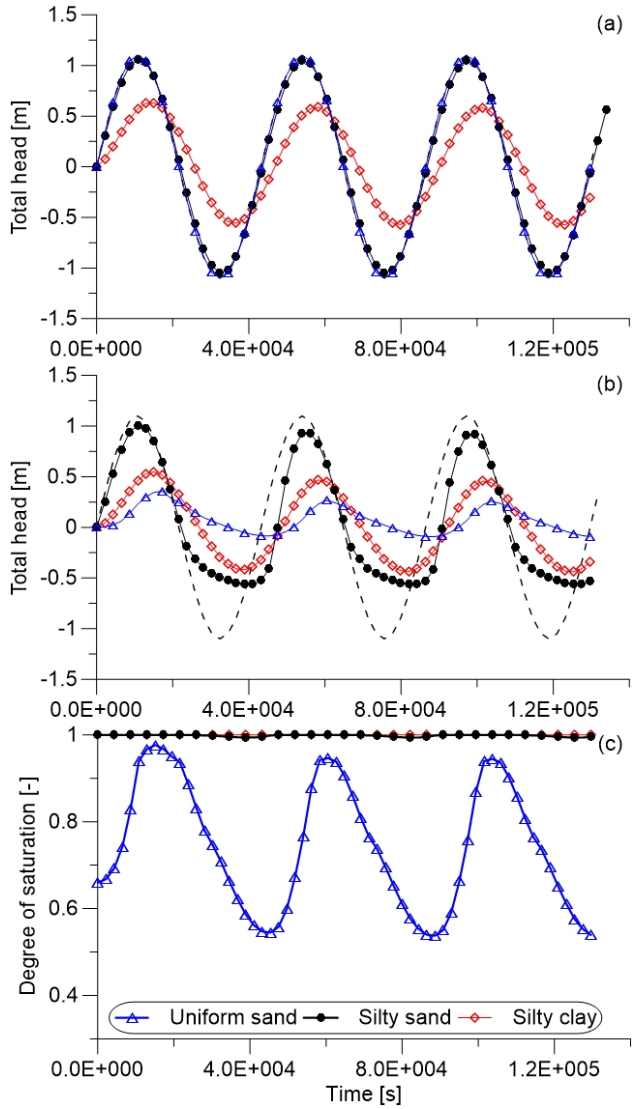

Fig 18. Total head and degree of saturation along time at x=10m, y=0.6m for different types of soils in (a) saturated conditions (1-SP-SAT, 1-SPML-SAT and 1-MLCL-SAT) and (b-c) unsaturated conditions (1-SP-UNSAT, 1-SPML-UNSAT and 1-MLCL-UNSAT).

Fig. 19 shows the variation of total head and degree of saturation for different boundary conditions for uniform sand (SP). Case 1 and 2 provide very similar results, because the total head does not exceed the level of the paving except at closer distance from the quay wall. The maximum infiltration rate in Case 2

is about 10^{-5} m/s, therefore the volume of water entering the square by seepage through soil may be considered small. When the paving is flooded, water infiltrates from the top rapidly increasing the degree of saturation and the total head; but when the sea level becomes lower than the paving elevation the response to tidal waves decreases significantly. Note that this behaviour is qualitatively similar to the measurements shown in Fig 9.

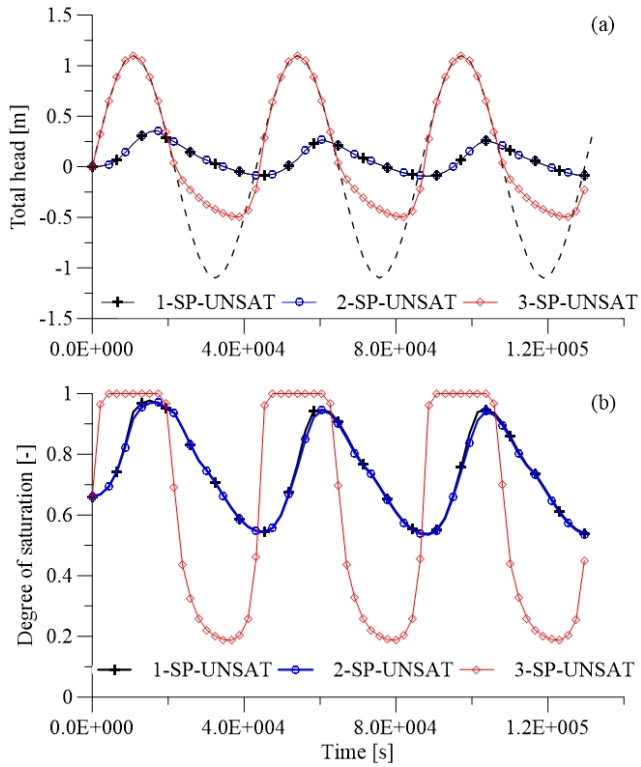

Fig 19. Total head (a) and degree of saturation (b) along time at x=10m, y=0.6m for 1-SP-UNSAT, 2-SP-UNSAT, 3-SP-UNSAT.

Infiltration from drainage network

In order to study the effects of water infiltrating into the ground from an ancient *gatolo* (i.e. the masonry of the lateral walls is pervious due to mortar degradation between the brick element), a model reproducing the geometry of a typical *gatolo* embedded in formation (1) has been considered, as shown in

Fig. 20: the homogeneous soil ranges between the elevation of y=+0.9 m and y=-2.0 m s.l.P.S., with a width of 40 m.

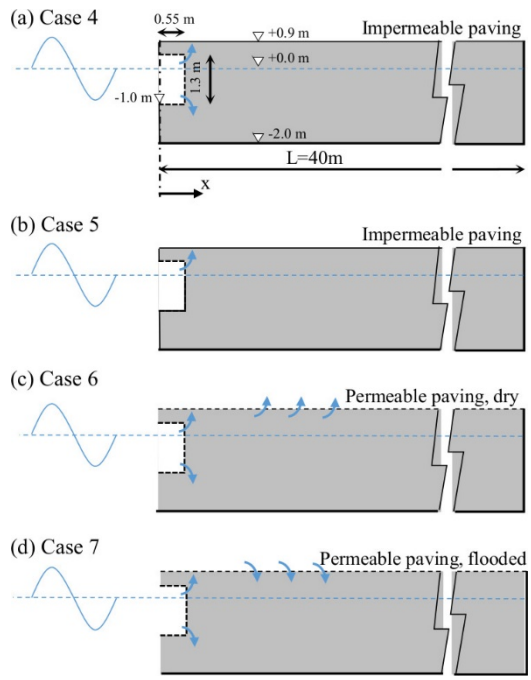

Fig 20. Geometry and boundary conditions of the models to study infiltration from gatolo (a) Case 4, (b) Case 5, (c) Case 6, (d) Case 7.

Table 3. Summary of numerical simulations considering infiltration from the gatolo

Boundary condition	Soil type	Saturated/Unsaturated	Simulation ID
Case 4	SP	Unsaturated	4-SP-UNSAT
	SP-ML	Unsaturated	4-SPML-UNSAT
	CL-ML	Unsaturated	4-CLML-UNSAT
Case 5	SP	Unsaturated	5-SP-UNSAT
	SP-ML	Unsaturated	5-SPML-UNSAT
	CL-ML	Unsaturated	5-CLML-UNSAT
Case 6	SP	Unsaturated	6-SP-UNSAT
	SP-ML	Unsaturated	6-SPML-UNSAT
	CL-ML	Unsaturated	6-CLML-UNSAT
Case 7	SP	Unsaturated	7-SP-UNSAT
	SP-ML	Unsaturated	7-SPML-UNSAT
	CL-ML	Unsaturated	7-CLML-UNSAT

To simulate water seepage from a permeable *gatolo*, the water level oscillation at the *gatolo*'s outer boundaries is assumed, in this context, to be the same as the tide level in the St. Mark's basin. Ancient *gatoli* are often partially filled by soil particles, due to silt and clay sedimentation occurring during the recurrent tidal inflow and outflow. In the numerical simulations, in cases 4, 6 and 7 the lateral walls are considered fully permeable (Fig. 20a, c and d, namely a clean *gatolo*), whereas case 5 is assuming the presence of a sediment deposit obstructing the seepage though the pervious walls only below a certain level, that is y=0.00 m s.l.P.S. (Fig. 20b). The boundary conditions on the top and bottom are assumed the same as in the previous section, being the square pavement impermeable (cases 4 and 5) or permeable, and in the latter case it can be dry (case 6) or flooded (case 7).

For each case shown in Fig. 20, three different types of soils have been considered (SP, SP-ML, CL-ML) in unsaturated conditions. This results in a total of 12 numerical simulations summarized in Table 3. The most important outcome of these parametric analyses is discussed in the following referring to uniform sand; however, similar conclusions can be drawn for other soil types.

With these models, bi-dimensional effects in pressure distribution can be appreciated as shown in Fig. 21, which plots the contours of the total head in the anthropic layer for cases 4-SP-UNSAT and 5-SP-UNSAT, considering a tidal wave of amplitude of 0.5 m.

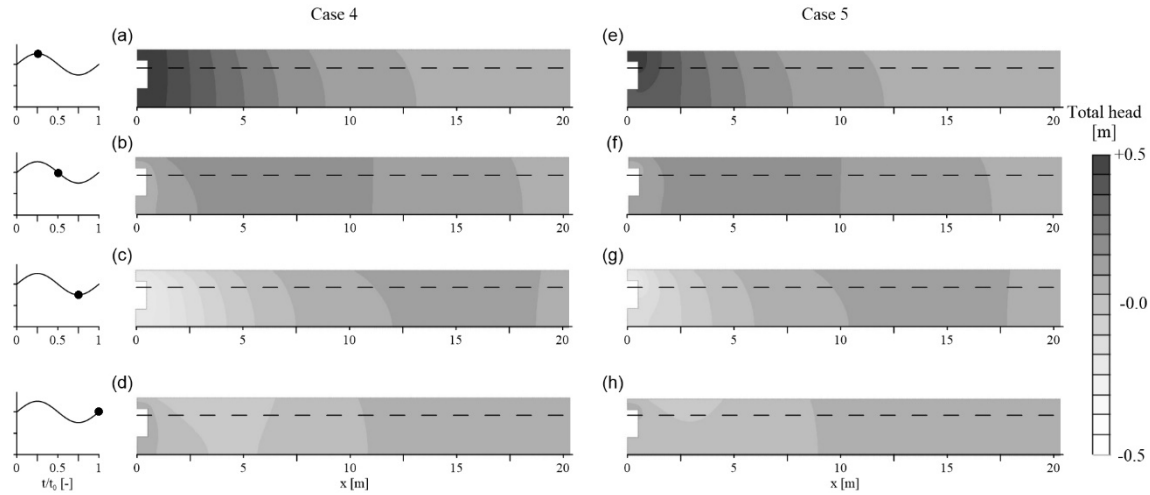

Fig 21. Contours of total head at significant time steps for case 4-SP-UNSAT (a-d) and 5-SP-UNSAT (e-f). (a,e) t/t_0=0.25, (b, f) t/t_0=0.5, (c, g) t/t_0=0.75, (d, h) t/t_0=1.0. For a better view only a length of 20m is shown.

The oscillation of pore pressure in soil has a similar trend as discussed in previous section: during increasing tidal level the response of the system is rapid, while the pore pressure dissipation is slower for decreasing water level. Delay and attenuation increases with distance and they are higher for uniform sand and lower for silty sand (Fig. 22).

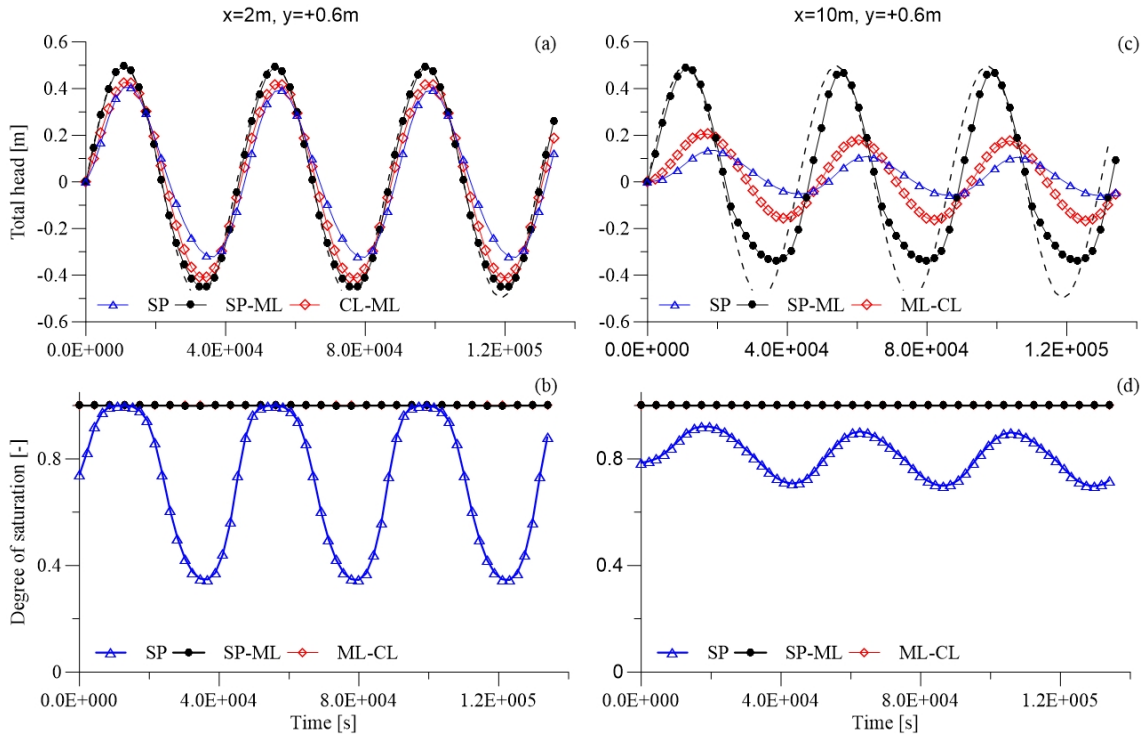

Fig 22. Total head (a, c) and degree of saturation (b, d) along time for case 1 and different types of soils, distance x=2m, y=+0.6m (a, b) and x=10m, y=+0.6m (c, d).

The effect of boundary condition at the top boundary (paving) is investigated considering an amplitude of tidal wave equal to 1.1 m and comparing cases 4, 6 and 7 (Fig. 20). The total head distribution is similar for case 4 and 6. In the latter, the maximum outflow rate in uniform sand at the paving level is about 10^{-5} m/s and decreases rapidly with distance; this means that the volume of water entering the square by seepage is small. The condition of flooded paving (case 7) produces a faster diffusion of the extreme pressure values (both positive and negative) within the layer (Fig. 23).

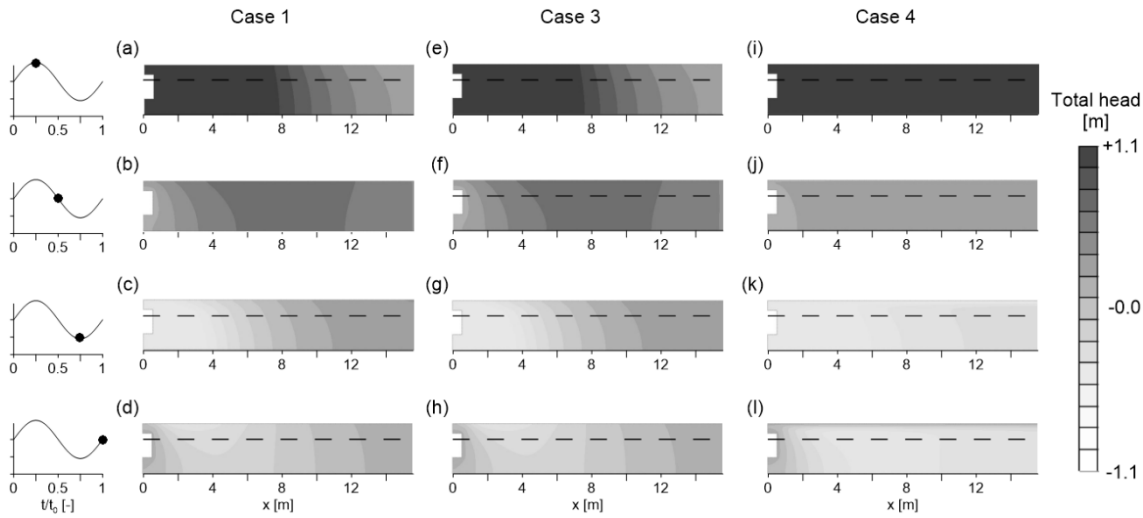

Fig 23. Contours of total head at significant time steps for 4-SP-UNSAT (a-d), 6-SP-UNSAT (e-h) and 7-SP-UNSAT (i-l). (a, e, i) t/t_0=0.25, (b, f, j) t/t_0=0.5, (c, g, k) t/t_0=0.75, (d, h, l) t/t_0=1.0. For a better view only a length of 15 m is shown.

SUMMARY AND CONCLUSIONS

The design of a cost-effective flood mitigation measure of St. Mark Square requires a multidisciplinary approach and the geotechnical study plays a fundamental role. Within this framework, this paper presents and discusses measurements and modelling of pore pressure oscillations in the soil of St. Mark's Square in Venice. The results provided important information to guide the design of the project and could be of interest for similar coastal problems.

The local soil profile is characterized by a heterogeneous alternation of layers composed of a mixture of sand, silt, and clay in different proportions. The pore pressure in formation 1 and 3 is clearly influenced by the sea water fluctuation. The local vertical component of hydraulic gradient between the two layers is directed downwards for higher tides and upwards for the lower ones. Thus infiltration from deeper layer is impossible during high tide peaks. In the shallower layer, maximum water levels are close to sea level, whereas the minimum ones are higher; moreover, pore pressure may stay higher than sea level during tide

decrease. This may be a key phenomenon to be considered when carrying uplift analyses of architectural elements as well as for the long term stability of paving especially in the more depressed area of St. Mark's Square.

A simple analytical one-dimensional solution can describe reasonably well the attenuation and delay of the tide oscillation in the upper layer close to the quay walls. However, partial soil saturation in the upper formation and different boundary conditions should be taken into account by means of finite element analyses. From all the numerical analyses carried out so far, it turns out that the effect of partial saturation and the type of soil cannot be neglected in the interpretation of field measurements, especially in the case of submerged paving. When soil is saturated the response of the system is rapid, while the decrease of pore pressure is slower in partially saturated conditions, giving an insight into the measured pore pressure response.

In the worst simulated condition for seepage rate, namely the top formation is entirely composed of uniform sand, the maximum outflow rate at the paving level is about 10^{-5}m/s and decreases rapidly with distance; this means that the volume of water entering the square by seepage is small. This information is particularly relevant for the retrofitting and improvement of the drainage system and for the design of the interventions to safeguard long term conservation of the St. Mark's Square.

ACKNOWLEDGMENTS

This work was supported by *Consorzio Venezia Nuova* [Prot. N. 14224 UGA/VA, 30/11/2018]. Moreover, the authors would like to thank the companies belonging to the Consortium *Kostruttiva*, in particular *Mate Eng*. and *Thetis*, and the colleagues of *ICEA* Department for the fruitful discussions regarding the flood protection of St. Mark's square.

REFERENCES

Aubertin, M., Mbonimpa, M., Bussière, B., and Chapuis, R. P. (2003). "A model to predict the water retention curve from basic geotechnical properties." *Canadian Geotechnical Journal*, 40(6), 1104–1122.

Barbieri, C., Di Giulio, A., Massari, F., Asioli, A., Bonato, M., and Mancin, N. (2007). “Natural subsidence of the Venice area during the last 60Myr.” *Basin Research*, 19(1), 105–123.

Bettiol, G., Ceccato, F., Pigouni, A. E., Modena, C., and Simonini, P. (2015). “Effect on the structure in elevation of wood deterioration on small-pile foundation: Numerical analyses.” *International Journal of Architectural Heritage*, 3058(November 2015).

Biscontin, G., Cola, S., Pestana, J. M., and Simonini, P. (2007). “Unified compression model for venice lagoon natural silts.” *Journal of Geotechnical and Geoenvironmental Engineering*, 133(8), 932–942.

Bortoletto, M. (2019). *Relazione archeologica - Interventi di salvaguardia dell’Insula di Piazza San Marco a Venezia*.

Carbognin, L., Teatini, P., Tomasin, A., and Tosi, L. (2010). “Global change and relative sea level rise at Venice: What impact in term of flooding.” *Climate Dynamics*, 35(6), 1055–1063.

Ceccato, F., Simonini, P., Koppl, C., Schweiger, H. F., and Tschuchnigg, F. (2014). “FE Analysis of degradation effects on the wooden foundations in Venice.” *Rivista Italiana di Geotecnica*, 2(2), 27–37.

Center, T. H. (2009). “Resilient Coasts : A Blueprint for Action.” *Resilient Coasts Initiative*.

Cola, S., Sanavia, L., Simonini, P., and Schrefler, B. a. (2008). “Coupled thermohydromechanical analysis of Venice lagoon salt marshes.” *Water Resources Research*, 44(5), n/a-n/a.

Cola, S., and Simonini, P. (2002). “Mechanical behavior of silty soils of the Venice lagoon as a function of their grading characteristics.” *Canadian Geotechnical Journal*, 39(4), 879–893.

CVN. (1998). “Project documentation.” Venice.

Favaretto, C., Martinelli, L., and Ruol, P. (2019). “Coastal flooding hazard due to overflow using a level II method: Application to the Venetian littoral.” *Water (Switzerland)*, 11(1).

Fletcher, C. A., and Spencer, T. (Eds.). (2005). *Flooding and environmental challenges for Venice and its lagoon: state of knowledge.* Cambridge University Press.

Fritz, H. M., Blount, C., Sokoloski, R., Singleton, J., Fuggle, A., McAdoo, B. G., Moore, A., Grass, C., and Tate, B. (2008). “Hurricane Katrina Storm Surge Reconnaissance.” *Journal of Geotechnical and Geoenvironmental Engineering*, 134(5), 644–656.

Horn, D. P. (2002). “Beach groundwater dynamics.” *Geomorphology*, 48(1–3), 121–146.

Jamiolkowski, M., Ricceri, G., and Simonini, P. (2009). “Safeguarding Venice from high tides: Site characterization & geotechnical problems.” *Proceedings of the 17th International Conference on Soil Mechanics and Geotechnical Engineering: The Academia and Practice of Geotechnical Engineering*, 3209–3227.

Monaco, P., Amoroso, S., Marchetti, S., Marchetti, D., Totani, G., Cola, S., and Simonini, P. (2014).

"Overconsolidation and stiffness of venice lagoon sands and silts from SDMT and CPTU." *Journal of Geotechnical and Geoenvironmental Engineering*, 140(1), 215–227.

Mualem, Y. (1976). "Hysteretical models for prediction of the hydraulic conductivity of unsaturated porous media." *Water Resources Research*, 12(6), 1248–1254.

P. Salandin. (2020). *Evaluation of flooding of the Sankt Mark's Island in: 'Analysis of possible interventions to safeguard the Sankt Mark's Island from high tides' Part 3 (in italian)*. Padova.

Penning-Rowsell, E. C., De Vries, W. S., Parker, D. J., Zanuttigh, B., Simmonds, D., Trifonova, E., Hissel, F., Monbaliu, J., Lendzion, J., Ohle, N., Diaz, P., and Bouma, T. (2014). "Innovation in coastal risk management: An exploratory analysis of risk governance issues at eight THESEUS study sites." *Coastal Engineering*, Elsevier B.V., 87, 210–217.

Ricceri, G. (2007). "Il ruolo della geotecnica nella salvaguardia della città di Venezia e della sua laguna."

Ricceri, G., Simonini, P., and Cola, S. (2002). "Applicability of piezocone and dilatometer to characteruze the soils of the Venice lagoon." *Geothchnical and Geological Engineering*, 20, 89–121.

Rinaldo, A., Nicotina, L., Alessi Celegon, E., Beraldin, F., Botter, G., Carniello, L., Cecconi, G., Defina, A., Settin, T., Uccelli, A., D'Alpaos, L., and Marani, M. (2008). "Sea level rise, hydrologic runoff, and the flooding of Venice." *Water Resources Research*, 44(12), 1–12.

Ruol, P., Favaretto, C., Volpato, M., and Martinelli, L. (2020). "Flooding of Piazza San Marco (Venice): Physical model tests to evaluate the overtopping discharge." *Water (Switzerland)*, 12(2).

Simonini, P., Ricceri, G., and Cola, S. (2007). "Geotechnical characterization and properties of Venice lagoon heterogeneous silts." *Characterisation and Engineering Properties of Natural Soils*, Leroueil and Hight, eds., Taylor & Francis Group, London, London, 2289–2327.

Di Sipio, E., and Zezza, F. (2011). "Present and future challenges of urban systems affected by seawater and its intrusion: The case of Venice, Italy." *Hydrogeology Journal*, 19(7), 1387–1401.

Sun, H. (1997). "A two-dimensional analytical solution of groundwater responses to tidal loading in an estuary and ocean." *Water Resources Research*, 33(6), 1429–1435.

Tonni, L., and Simonini, P. (2013). "Shear wave velocity as function of cone penetration test measurements in sand and silt mixtures." *Engineering Geology*, Elsevier B.V., 163, 55–67.

Turner, I. L. (1998). "Monitoring groundwater dynamics in the littoral zone at seasonal, storm, tide and swash frequencies." *Coastal Engineering*, 35(1–2), 1–16.

Turner, I. L., Coates, B. P., and Acworth, R. I. (1997). "Tides, waves and the super-elevation of groundwater at the coast." *Journal of Coastal Research*, 13(1), 46–60.

Ursino, N., Silvestri, S., and Marani, M. (2004). "Subsurface flow and vegetation patterns in tidal environments." *Water Resources Research*, 40(5), 1–11.

Volpato, M. (2019). *Relazione idrologica e idraulica - Interventi di salvaguardia dell'Insula di Piazza San Marco a Venezia*. Venice.

Vousdoukas, M. I., Mentaschi, L., Feyen, L., and Voukouvalas, E. (2017). "Extreme sea levels on the rise along Europe's coasts." *Earth's Future*, 5(3), 1–20.

Zanuttigh, B. (2011). "Coastal flood protection: What perspective in a changing climate? The THESEUS approach." *Environmental Science and Policy*, 14(7), 845–863.

Zanuttigh, B., Nicholls, R., and Hanson, S. (2014). *Introduction*. *Coastal Risk Management in a Changing Climate*, Elsevier Inc.